Polysarcosine-based lipid formulations for intracranial delivery of mRNA

Bi, D.; Unthan, D.M.; Hu, L.; Bussmann, J.; Remaut, K.; Barz, M.; Zhang, H.

Journal of Controlled Release 356 (2023) 1–13

Contents lists available at ScienceDirect

Journal of Controlled Release

journal homepage: www.elsevier.com/locate/jconrel

Polysarcosine-based lipid formulations for intracranial delivery of mRNA

Dongdong Bi [a,1], Dennis Mark Unthan [a,1], Lili Hu [a], Jeroen Bussmann [a], Katrien Remaut [b], Matthias Barz [a,c,*], Heyang Zhang [a,*]

[a] Leiden Academic Centre for Drug Research (LACDR), Leiden University, Einsteinweg 55, 2333, CC, Leiden, the Netherlands
[b] Laboratory for General Biochemistry and Physical Pharmacy, Faculty of Pharmaceutical Sciences, Ghent University, 9000 Ghent, Belgium
[c] Department of Dermatology, University Medical Center of the Johannes Gutenberg University Mainz, Langenbeckstraße 1, 55131 Mainz, Germany

ARTICLE INFO

Keywords:
Polysarcosine
Lipid formulations
mRNA intracerebral delivery
Zebrafish embryo

ABSTRACT

Messenger RNA (mRNA) is revolutionizing the future of therapeutics in a variety of diseases, including neurological disorders. Lipid formulations have shown to be an effective platform technology for mRNA delivery and are the basis for the approved mRNA vaccines. In many of these lipid formulations, polyethylene glycol (PEG)-functionalized lipid provides steric stabilization and thus plays a key role in improving the stability both *ex vivo* and *in vivo*. However, immune responses towards PEGylated lipids may compromise the use of those lipids in some applications (*e.g.*, induction of antigen specific tolerance), or within sensitive tissues (*e.g.*, central nervous system (CNS)). With respect to this issue, polysarcosine (pSar)-based lipopolymers were investigated as an alternative to PEG-lipid in mRNA lipoplexes for controlled intracerebral protein expression in this study. Four polysarcosine-lipids with defined sarcosine average molecular weight (M_n = 2 k, 5 k) and anchor diacyl chain length (m = 14, 18) were synthesized, and incorporated into cationic liposomes. We found that the content, pSar chain length and carbon tail lengths of pSar-lipids govern the transfection efficiency and biodistribution. Increasing carbon diacyl chain length of pSar-lipid led up to 4- and 6-fold lower protein expression *in vitro*. When the length of either pSar chain or lipid carbon tail increased, the transfection efficiency decreased while the circulation time was prolonged. mRNA lipoplexes containing 2.5% C14-pSar2k resulted in the highest mRNA translation in the brain of zebrafish embryos through intraventricular injection, while C18-pSar2k-liposomes showed a comparable circulation with DSPE-PEG2k-liposomes after systemic administration. To conclude, pSar-lipid enable efficient mRNA delivery, and can substitute PEG-lipids in lipid formulations for controlled protein expression within the CNS.

1. Introduction

Neurological diseases are a leading cause of disability and the second most important factor for global mortality [1]. Messenger RNA (mRNA), as a new drug class, has been extensively investigated in a range of applications, including vaccines, protein replacement therapies, cancer immunotherapies, genome editing, *etc.* [2]. However, research on mRNA therapy to treat neurological disorders is still rather limited due to the inherent susceptibility and immunogenicity of mRNA as well as the existence of blood-brain barrier (BBB) and the anatomical structure of the brain [3]. On one hand, efforts have been made to enhance mRNA stability and fine-tune the mRNA-induced immune stimulation, such as chemical modification and purification. On the other hand, continuous attention has been paid on the development of safe and efficacious delivery methods for mRNA. For example, Yuta et al. intraventricularly injected mRNA encoding brain-derived neurotrophic factor and found a significant improvement in the survival rate of rats with brain ischemia [4]. Peng et al. also reported that intracranial injection of mRNA complexed by either TransIT or *in vivo*-jetPEI led to a notable antitumor effect in a mouse glioma model [5]. Despite the remarkable advances in lipid-based mRNA delivery, safe and efficient formulations are urgently needed to unleash the full potential of mRNA therapeutics for neurological disorders. Among nanocarriers that are currently suitable to intracerebral mRNA delivery, liposomes have attracted increasing attention to enable functional mRNA transfer across the BBB [5–8]. They can be administrated through systemic injection or local injection. Given the limited efficacy of mRNA transfer across the barriers of the central nervous system (CNS), the local administration of lipid formulations

* Corresponding authors.
E-mail addresses: m.barz@lacdr.leidenuniv.nl (M. Barz), h.zhang@lacdr.leidenuniv.nl (H. Zhang).
[1] Dongdong Bi and Dennis Mark Unthan contributed equally to this work.

https://doi.org/10.1016/j.jconrel.2023.02.021
Received 31 August 2022; Received in revised form 5 January 2023; Accepted 14 February 2023
Available online 28 February 2023

exhibits several advantages including lower therapeutic dose and reduced adverse effects [9]. A recent Phase 1 study has demonstrated that it is safe to inject stem cells into the human intracerebral ventricular [10]. Also, a clinical trial is currently ongoing to investigate rhenium-containing liposome formulations for local injection in the treatment of brain tumors (clinicaltrails.gov NCT01906385) which underlines the potency of local injections of lipid formulations to the CNS [7].

Polyethylene glycol (PEG), a hydrophilic and biocompatible polymer, is widely used to modify the surface of nanoparticles to improve the stability in solution by steric repulsion, and to prolong systemic circulation time by reducing the recognition and clearance *via* reticuloendothelial system (RES). To date, five PEGylated lipid formulations including Doxil, Onivyde, Onpattro, Comirnaty, Spikevax, have received FDA approval in the clinic [11]. For example, Comirnaty and Spikevax contain 1.5 mol% ALC-0159 and DMG (dimyristoyl glycerol)-PEG2k respectively. 5.0 mol% and 0.3 mol% DSPE (distearyl phosphatidylethanolamine)-PEG2k was applied into liposomal Onivyde and Doxil, respectively [12,13]. Currently, PEG-associated toxicological and immunological concerns have received considerable attention because of the hypersensitivity reactions (*e.g.*, anaphylaxis) after administration of the approved mRNA COVID-19 vaccines based on PEGylated lipid nanoparticles (LNPs) [14–16]. Of note, the accelerated blood clearance (ABC) phenomenon has been additionally reported for a variety of PEGylated nanoparticles (*e.g.*, PEG chain length and surface density), likely due to the presence of anti-PEG IgM in many patients [17]. The ABC phenomenon leads to a rapid clearance of administrated PEGylated nanoparticles, which compromises the required therapeutic doses, needs repeated administrations and therefore may increase adverse effects [18–20]. To address the aforementioned PEG dilemma, efforts have been placed to abrogate the immunogenicity of PEGylated formulations without significant impairment of shielding effects, such as optimizing surface density of PEGylation on particles, the use of sheddable PEG (*e.g.*, DMG-PEG2k) and PEG alternatives (*e.g.*, polyglycerols, polyoxazolines, polysarcosine) [20–25].

Polysarcosine (pSar) is a polypeptoid derived from the endogenous amino acid sarcosine (*N*-methylated glycine), and exhibits comparable stealth-like properties to PEG both *in vitro* and *in vivo* [26–28]. More importantly, a low immunogenicity of pSar-lipids in both rabbits and rats or even an absence of any immediate immune response in zebrafish and mice was found [29,30]. The applicability of pSar-modified lipids has been extended to mRNA LNPs, and led to an improved protein expression and a reduced immunostimulatory response after systemic administration compared to PEGylated LNPs, implying pSar as a safe and potent substitute of PEG [31]. Typically, PEG is incorporated into lipid formulations through covalent conjugation with lipids, such as DMG, DSPE, and 1,2-dioleoyl-sn-glycero-3-phosphoethanolamine (DOPE), to tackle the shortcomings associated with new molecular entities with suboptimal biopharmaceutical attributes, and to maintain PEG staying on the surface of nanoparticles [32]. Similar to PEGylated lipids, the diacyl groups act as anchor for integration in the lipid formulation, and the pSar chains localize towards the aqueous environment [33]. Together with pSar chain length and surface density of pSar, the diacyl chain length and architecture affect the physicochemical properties (*e.g.*, size, membrane fluidity, stability) and biological performance (*e.g.*, circulation time, biodistribution, cellular uptake) of particles [34–37].

In the present study, we report the development of a cationic liposomes-based mRNA formulation based on a pSar-lipid shielding to achieve functional mRNA transfer to the CNS *via* intraventricular injection. First, pSar-lipid with varying of sarcosine repeating unit (M_n = 2 k, 5 k) and lipid tail length (m = 14, 18), were synthesized and characterized. Then, pSar-lipid with varying molar fractions (2.5, 5.0, 10%) was applied into liposomes comprising of DOTAP and DOPE, to study the influence of content, alkyl chain length and pSar chain length of pSar-lipid on the physicochemical properties. PEGylated lipids were used as internal control to relate the observed efficacy of pSar-based lipoplexes to established systems. We used *in vitro* cellular uptake and transfection studies to preliminarily screen the formulations. Next, zebrafish embryos were employed to study the translation of mRNA lipoplexes from *in vitro* to *in vivo*. The biodistribution of various pSar-based cationic liposomes were observed through intravenous injection and compared with PEG-based liposomes. The transfection effect of selected mRNA lipoplexes, and toxicity of lipoplexes were studied in zebrafish embryo to compare pSar- and PEG-based nanoparticles.

2. Materials & methods

2.1. Materials

Unless stated otherwise, reagents and solvents were purchased from Sigma Aldrich (Zwijndrecht, The Netherlands) and used as received. Benzonitrile was dried over CaH_2, distilled and stored over activated molecular sieve (3 Å) prior to use. Toluene used for polymerizations was purchased from Thermo Scientific (99.85%, Extra Dry over Molecular Sieve, AcroSeal®, Landsmeer, The Netherlands). Milli-Q water was prepared using a MILLI-Q® Reference A+ system. Water was used at a resistivity of 18.2 MΩ/cm and total organic carbon <5 ppm. Hexafluoroisopropanol (HFIP) and potassium trifluoroacetate were purchased from Fluorochem. Deuterated solvents were purchased from Deutero GmbH and were used as received. All lipids were purchased from Avanti Polar Lipids (Alabaster, AL, USA) and stored at −20 °C in lyophilized form or rehydrated in chloroform. Chemically modified messenger RNA encoding enhanced Green Fluorescence Protein (GFP, for *in vitro* test) and chemically modified mRNA encoding luciferase that was labeled by Atto 488 (for *in vivo* release study) were provided by TRON-Translational Oncology at the University Medical Center of the Johannes Gutenberg University Mainz GmbH (Mainz, Germany) and PureBoost™ GFP mRNA was kindly provided by Cellerna Bioscience (Baesweiler, Germany) for *in vivo* studies. HEPES, sodium dodecyl sulfate, chloroform, Tris-base, boric acid, sodium azide, EDTA and D-(+)-glucose were purchased from Sigma-Aldrich (Zwijndrecht, The Netherlands). UltraPure™ agarose, Lipofectamine™ 2000, trypan blue (0.4%), bovine serum albumin, Hoechst 33342, trypsin/EDTA and Dulbecco's Modified Eagle's Medium/F12 (DMEM/F12) were purchased from Thermo Fisher Scientific (Landsmeer, The Netherlands). RPMI1640, L-glutamine, PEN-STREP (10,000 U/mL penicillin, 10,000 U/mL streptomycin) and DPBS (without Ca^{2+} or Mg^{2+}) were bought from Lonza Bioscience (Verviers, Belgium). Gelred was bought from Bioconnect (Huissen, The Netherlands). Fetal bovine serum was purchased from SERANA (Brandenburg, Germany).

3. Methods

^{1}H NMR spectra were recorded on a Bruker Avance II 400 at room temperature at a frequency of 400 MHz. DOSY spectra were recorded on a Bruker Avance III HD 500 (500 MHz). Calibration of the spectra was achieved using the solvent signals. NMR spectra were analyzed with MestReNova version 12.0.4 from Mestrelab Research S.L. Degrees of polymerization (X_n) by ^{1}H NMR were calculated by comparing the integral of the initiator peak and the integrals of the α-protons. Attenuated total reflectance Fourier transform infrared (ATR-FT-IR) spectroscopy was performed on a FT/IR-4100 (JASCO Corporation) with an ATR sampling accessory (MIRacle, Pike Technologies). IR spectra were analyzed using Spectra Manager 2.0 (JASCO Corporation). Completion of the N-carboxyanhydride (NCA) polymerization was monitored by FT-IR spectroscopy by the disappearance of the NCA related carbonyl bands at 1853 cm^{-1} and 1786 cm^{-1}. Analytical gel permeation chromatography (GPC) was performed on a Jasco GPC setup at a flow rate of 1.0 mL/min, 40 °C. The eluent was HFIP equipped with 3 g/L potassium trifluoroacetate. The column material was a modified silica gel (PFG columns; particle size, 7 μm; porosity, 100 and 4000 Å), purchased from PSS Polymer Standards Service GmbH. For polymer detection, a UV

detector (Jasco UV-2075+) at a wavelength of λ = 230 nm was employed. Molecular weights were determined by using a calibration with PMMA (PSS Polymer Standards Services GmbH) with toluene as an internal standard. The elution diagram was evaluated with PSS WinGPC (PSS Polymer Standards Service GmbH).

3.1. Initiator synthesis

3.1.1. Di-N-Tetradecylamine

Di-*N*-tetradecylamine was synthesized according to literature [38]. A solution of tetradecylamine (5.0 g, 23.4 mmol, 1.0 eq), DMAP (430 mg, 3.5 mmol, 0.15 eq) and NEt_3 (4.9 mL, 35.1 mmol, 1.5 eq) in 60 mL Toluene was cooled to 0 °C and a solution of myristoyl chloride (5.8 g, 23.4 mmol, 1.0 eq) in 50 mL Toluene was added dropwise. The solution was stirred at room temperature for two days, the solvent removed, and the residue recrystallized twice from EtOH and dried *in vacuo*. This product (6.74 g, 15.9 mmol) was dissolved in 40 mL anhydrous THF and a suspension of $LiAlH_4$ in 30 mL anhydrous where THF was carefully added. The reaction was refluxed for 18 h, then cooled to room temperature and poured into 300 mL 10% aq. Na_2SO_4, 300 mL $CHCl_3$ was added, the mixture stirred and filtered. The solid was washed with $CHCl_3$, the filtrates combined, and the organic phase washed with brine and evaporated. The residue was recrystallized from EtOH. Yield: 6.31 g (71%).

^{1}HNMR(400MHz,$CDCl_3$,δ):0.87(6H,t),1.24(44H,m),1.48(4H,t),2.57(4H,t)

3.2. Monomer synthesis

3.2.1. Sarcosine N-carboxy anhydride

The synthesis approach was adapted from literature [39–41]. A total of 14.92 g (167.4 mmol) sarcosine, dried under vacuum for 1 h, was weighed into a pre-dried, three neck, round-bottom flask. A total of 300 mL of absolute THF was added under a steady flow of nitrogen, 16.2 mL (134 mmol) of diphosgene was added slowly *via* syringe, and the nitrogen stream was reduced. The colourless suspension was mildly refluxed for 3 h, yielding a clear solution. Afterward, a steady flow of dry nitrogen was led through the solution for another 3 h while the outlet was connected to two gas washing bottles filled with aqueous NaOH solution to neutralize phosgene. The solvent was evaporated under reduced pressure, yielding a brownish oil as a crude reaction product. The oil was dried under reduced pressure (1×10^{-3} mbar for 2 h) to obtain an amorphous solid, free of phosgene and HCl, confirmed by testing against a silver nitrate solution. The crude product was redissolved in 40 mL of THF and precipitated with 300 mL of dry n-hexane. The solution was cooled to −18 °C and stored for 18 h to complete precipitation. The solid was filtered under dry nitrogen atmosphere and dried in a stream of dry nitrogen for 60–90 min and afterward under high vacuum for 2 h in the sublimation apparatus. The crude product was sublimated at 85 °C and 1×10^{-3} mbar. The product was collected from the sublimation apparatus in a glovebox on the same day. The purified product (110 mmol, 65.0% yield, colourless crystallites; melting point: 102–104 °C (lit: 102–105 °C)) was stored in a Schlenk tube at −80 °C.

^{1}H NMR (400 MHz, $CDCl_3$, δ) : 2.86 (3H, s), 4.22 (2H, s)

3.2.2. Azidobutyric Acid Pentafluorphenylester

γ-Azidobutyric acid (7.74 mmol) was dissolved in pre-dried THF, and triethylamine (15.0 mmol, 2 equiv) was added. The solution was stirred at room temperature for 30 min. Then, two equivalents of pentafluorophenol trifluoroacetate (15.0 mmol) were added dropwise. The reaction mixture was stirred overnight at RT. Completion of the reaction was evaluated with thin-layer chromatography. THF was distilled, and the remaining solid was first dissolved in dichloromethane and then was extracted three times with water. The organic phase was dried with $MgSO_4$, and dichloromethane was distilled off the product. The product was purified by column chromatography (10:1 cyclohexane: ethyl acetate).

^{1}H NMR (400 MHz, $CDCl_3$, δ) : 2.04 (2H, q), 2.80 (2H, t), 3.46 (2H, t)

3.3. Polymer synthesis

3.3.1. BA_{C18}-polysarcosine-Azide

Dioctadecylamine was weighed in in a pre-dried Schlenk tube and dissolved in dry toluene to yield a solution of 10 mg/mL and heated to 50 °C. Sarcosine NCA was dissolved in dry benzonitrile (c = 100 mg/mL) and n equivalents of sarcosine NCA was added to the initiator solution. The solution was stirred at 50 °C. Completion of the reaction was confirmed by Fourier transform infrared (FT-IR) spectroscopy by monitoring the disappearance of the NCA related peaks at 1853 and 1786 cm^{-1}. Then, the sarcosine amino termius was quenched with the addition of 5 equivalents of dry triethylamine and 5 equivalents of azidobutyric acid pentafluorophenyl ester. The clear reaction mixture was stirred at room temperature overnight followed by the addition of 5 equivalents of acetic anhydride to react with any residual end groups. The reaction mixture was stirred at room temperature for another day. The polymer was then precipitated in cold diethyl ether and centrifuged (4500 *g* at 4 °C for 15 min). After discarding the liquid fraction, new ether was added, and the polymer was resuspended in a sonication bath. The suspension was centrifuged again, and the procedure repeated. The polymer was dissolved in water and dialyzed against MilliQ water and lyophilized, obtaining a colourless, stiff and porous solid.

^{1}H NMR (500 MHz, DMSO-d_6,δ) : 0.85 (6H, t), 1.06–1.33 (64H, m), 1.37 –1.60 (4H, m), 1.64–1.81 (2H, m), 2.59–3.04 (3n H, m), 3.74–4.49 (2n H, m)

3.3.2. BA_{C14}-polysarcosine-Azide

BA_{C14}-polysarcosine-Azide was synthesized accordingly.

3.4. Liposome preparation

Lipid composition and molar ratio of formulations is shown in SI Table 1. All liposomes were prepared by lipid film hydration and extrusion method. Briefly, lipids were dissolved in ethanol, followed by evaporation under vacuum. The lipid film was hydrated with HEPES buffer (10 mM, pH 7.4) for 30 min at 30 °C. Liposomes were subsequently extruded with 400 nm and 100 nm polycarbonate filters for three times (Nucleopore Milipore, Kent, UK) by Lipex extruder (Northern Lipids Inc., Canada).

3.5. mRNA lipoplexes preparation

According to the desired N/P ratios, liposome and mRNA stock solutions were first diluted with HEPES buffer (10 mM, pH 7.4), Next, equal volume of mRNA and liposome were mixed well and incubated at room temperature for 5 min prior to use. The resulting lipoplexes were used as such, without any further washing or dialysis.

3.6. Size and ζ potential characterization

The average size and ζ potential of blank liposomes and mRNA lipoplexes were measured by using a Zetasizer Ultra (Malvern, Worcestershire, UK) in HEPES buffer (10 mM, pH 7.4). Blank liposomes were diluted with HEPES buffer to a final concentration of 100 μM for DLS measurement, and mRNA lipoplexes were measured at a final concentration of 0.25 μg/mL.

3.7. Complexation of mRNA lipoplexes

The ability of liposomes to complex mRNA was studied using 1.2%

agarose gel electrophoresis. Lipoplexes of mRNA/liposomes were prepared as described above. Briefly, 7.5 μL mRNA (150 ng) and 7.5 μL liposomes (with varying concentrations) were mixed, according to the defined N/P ratios. Free/naked mRNA with same amount (150 ng) was used as control. After 30 min' incubation at room temperature, 5 μL glucose (50%, *w/v*) was transferred to each sample before loading onto the gel. Gel electrophoresis was performed at 100 V for 30 min. Images were analyzed by Fiji Image J software.

3.8. In vitro biological performance

3.8.1. Cell culture

HeLa cells were cultured in DMEM/F12 with 10% Fetal Bovine Serum (FBS), 2 mM L-glutamine and 100 μg/mL penicillin/streptomycin at 37 °C, 5.0% CO_2. Cells with 80–90% confluency were detached from the bottom of the flask with 0.25% trypsin/EDTA. Jurkat T cells were cultured in RPMI1640 medium supplemented with 10% FBS, 2 mM L-glutamine and 100 μg/mL penicillin/streptomycin and maintained in a humidified atmosphere of 37 °C, 5.0% CO_2. The culture medium was renewed every 2–4 days. For all *in vitro* tests, Hela cells were seeded in 96-well F-bottom plates (Greiner Bio-one, Alphen aan den Rijn, The Netherlands) at a density of 15,000 cells/well. Jurkat T cells were seeded in each well of 96-well U-bottom plates (Greiner Bio-one, Alphen aan den Rijn, The Netherlands) at a density of and 40,000 cells/well. Cells were incubated at 37 °C, 5.0% CO_2 one day before treatment.

3.8.2. Biological performance

18:1 Liss Rhodamine PE (PE-LR) labeled liposomes were utilized to complex GFP mRNA at N/P ratio of 5, 10 and 20, as described above. In each well, 20 μL lipoplexes of liposome/mRNA (containing 0.2 μg mRNA) were transferred to the cells cultured in fresh culture medium with a final volume of 200 μL. After 24 h' incubation at 37 °C, 5.0% CO_2, Hela cells were rinsed with DPBS twice, trypsinized and collected by centrifugation at 500 *g* for 5 min, while Jurkat T cell pellet was harvested after washing with DPBS twice and subsequent centrifugation at 500 *g*, 5 min. 200 μL flow buffer (1% Bovine Serum Albumin, 0.1% NaN_3, DPBS[−]) was added to each well to resuspend cell pellets for measurements by flow cytometry (Cytoflex, Beckman Counter, Woerden, The Netherlands), to quantify the cellular uptake or protein expression.

3.9. In vivo biological performance

Zebrafish (*Danio rerio*) were maintained and handled according to the guidelines from the Zebrafish Model Organism Database (http://zfin.org) and in compliance with the directives of the local animal welfare committee of Leiden University. Fertilization was performed by natural spawning at the beginning of the light period, and eggs were raised at 28.5 °C in egg water (60 μg/mL Instant Ocean sea salts). Needles used for injection were prepared by pulling on a filamentary borosilicate capillary on a micropipette puller (P-97, Sutter Instruments). Femtojet (Eppendorf) pump was used for microinjection. Confocal z-stacks were captured on a Leica TCS SP8 confocal microscopy, using either a 10× air objective (HCX PL FLUOTAR) or a 40× water-immersion objective (HCX APO L). Laser intensity, gain, and offset settings for stacks and sessions were identical. Images were processed by using the Fiji Image J software.

3.9.1. In vivo protein expression

1.5 nL lipoplexes containing 150 pg of GFP mRNA was injected into the brain or duct of Cuvier of 2.5 dpf (days-post fertilization) wildtype (ABTL) zebrafish embryos ($n = 20$ in each group). To quantify the GFP expression, six zebrafish embryos were randomly chosen and examined using confocal microscopy. A direct comparison was made by counting the number of GFP-expressing cells in zebrafish brain to reflect the transfection efficiency of mRNA lipoplexes. Unless stated otherwise, all the mRNA lipoplexes that were injected into zebrafish embryos were prepared at N/P 10.

3.9.2. Biodistribution

Tg(*kdrl*:GFP)^{s843} zebrafish line with GFP expression in endothelial cells, was utilized to visualize the biodistribution of liposomes [42]. Embryos were anesthetized in 0.01% tricaine and embedded in 0.4% agarose gel containing tricaine before injection. 1 nL of PE-LR labeled liposomes (30 mM) was injected into 2.5 dpf zebrafish embryos. Then, embryos were removed from the agarose. At indicated timepoints (1 h, 5 h and 24 h) after injection, embryos were embedded again and imaged using confocal microscopy.

3.9.3. In vivo trafficking of mRNA lipoplexes

Atto488 labeled mRNA encoding luciferase was complexed by PE-LR labeled liposomes into lipoplexes at N/P 10. 1.5 nL lipoplexes (150 pg mRNA) was intravenously injected in 2.5 dpf ABTL zebrafish embryos. The behavior of mRNA lipoplexes was visualized by confocal microscopy at 1 h, 2 h, 4 h and 24 h post-administration.

3.9.4. In vivo toxicity

1.5 nL pSar-lipid or DSPE-PEG2k-containing liposomes (30 mM) was intravenously injected through duct of Cuvier or intracerebral injection into wildtype zebrafish embryos (2.5 dpf, $n = 20$ in each group). The appearance, behavior and mortality of zebrafish embryos were monitored for three days for toxicity evaluation.

3.10. Statistical analysis

Results are shown as mean ± standard deviation. Experiments were performed at least in triplicate on independent days. Significance between the means of two groups was tested using 2-way ANOVA with the software GraphPad Prism 7. Asterisks indicate statistical significance: * $p < 0.05$; ** $p < 0.01$; *** $p < 0.001$, **** $p < 0.0001$.

4. Result & discussion

4.1. Synthesis and characterization of pSar-lipids

First, different polysarcosine (pSar)-lipopolymers (pSar-lipids) with different molecular weight in the pSar block and alkyl chain lengths (C14 and C18) in the lipid-like part, were synthesized *via* controlled living ring opening polymerization of sarcosine NCA. The synthesis was performed according to our previously reported method (Fig. 1, A) [43]. Sarcosine N-carboxyanhydride (NCA) was synthesized and purified prior to use by sublimation and recrystallization ensuring a melting point of 105 °C and the absence of chloride impurities. Dioctadecylamine or tetradecylamine was used as an initiator for the polymerization of sarcosine NCA and subsequently end-capped with triethylamine and azidobutyric acid pentafluorophenyl ester. The pSar chain length of BA_{C18}-$pSar_{30}$-Azide was determined by ^{1}H NMR (Fig. 1, B). Further, ^{1}H DOSY NMR analysis underlined the presence of a single diffusing species, without any free initiator or side products (Fig. 1, C). All other pSar-lipids were characterized accordingly (SI Fig. 1). Analysis by gel permeation chromatography (GPC) in hexafluoroisopropanol (HFIP) displays lipopolymers with narrow, symmetric and monomodal molecular weight distributions with low dispersities ($Đ = 1.08–1.11$). A distinctive shift in the elution volume to higher molecular weights was detected by GPC, indicating the successful controlled living polymerization (Fig. 1, D). The incorporated azide end groups can be further modified by antibody or ligands to achieve active targeting effects using established protocols [44]. For ease of description, BA_{C14}-$pSar_{36}$-Azide, BA_{C14}-$pSar_{77}$-Azide, BA_{C18}-$pSar_{30}$-Azide, and BA_{C18}-$pSar_{65}$-Azide are abbreviated as C14-pSar2k, C14-pSar5k, C18-pSar2k, and C18-pSar5k according to their average molecular weight (M_n), respectively. Based on the report by Weber et al., the hydrodynamic volume of PEG and pSar

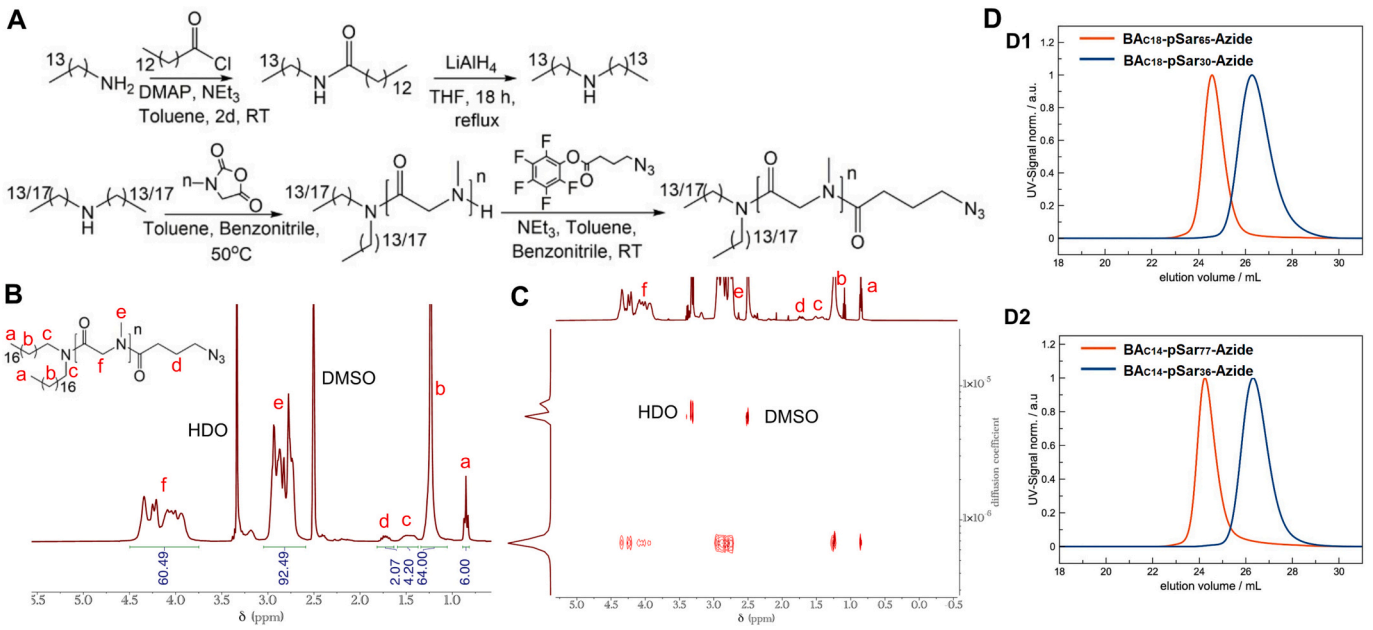

Fig. 1. (A) Polymerization of sarcosine NCA with dioctadecyl/tetradecylamine as initiator followed by end-capping with azidobutyric acid pentafluorophenylester. BA_{C18}-$pSar_{30}$-Azide was characterized by (B) ^{1}H NMR in DMSO-d_6, and (C) ^{1}H DOSY NMR in DMSO-d_6. (D) Analytical gel permeation chromatography in HFIP of (D1) BA_{C18}-$pSar_n$-Azide (n = 30, 65) and (D2) BA_{C14}-$pSar_n$-Azide (n = 36, 77).

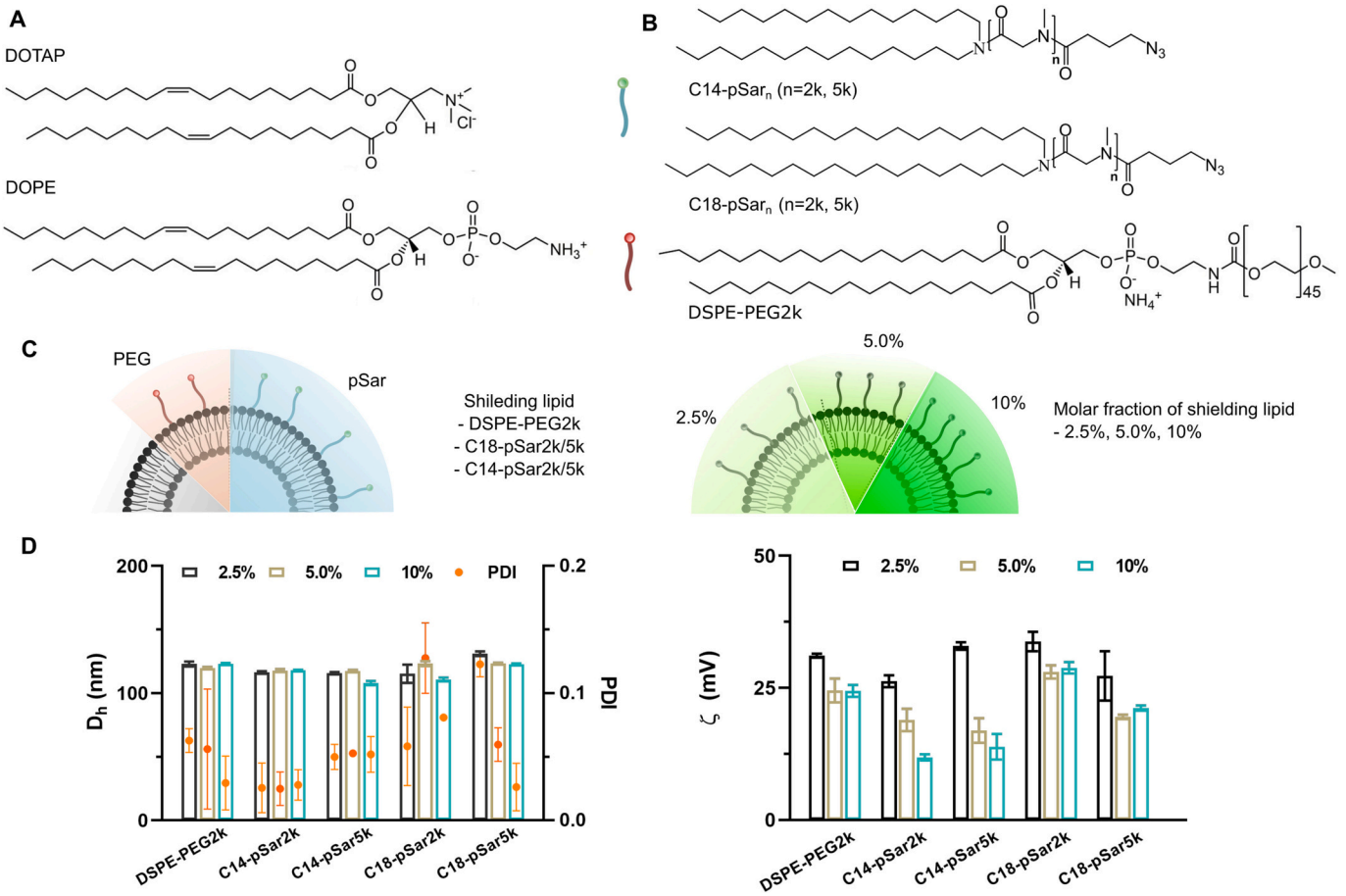

Fig. 2. (A-C) Schematic of liposomes comprising of (A) DOTAP, DOPE with shielding lipid, either (B) pSar-lipid or DSPE-PEG2k at different molar fraction. (D) Hydrodynamic diameter and ζ potential of liposomes in HEPES buffer (10 mM, pH 7.4) were determined by DLS (n = 3).

calculated by average molecular weight and not by degree of polymerization [28].

4.2. pSar-lipid affected the physicochemical properties of liposome in a comparable manner to PEG-lipid

Next, pSar-lipids with varying sarcosine chain length (M_n = 2 k, 5 k) and alkyl chain length (C14, C18), at different molar fraction were incorporated into cationic liposomes comprising of DOTAP, 18:1 Liss Rhodamine PE (PE-LR), and the neutral lipid DOPE by using the thin-film hydration followed by extrusion. DSPE-PEG2k was used for comparison and as internal control. As reported before by Viitala et al., 0.5–10% PEGylated lipids did not affect the structural stability of the phospholipid bilayer of liposomes [45]. Therefore, 2.5%, 5.0% and 10% pSar-lipids or DSPE-PEG2k was used to achieve surface modification in this study. Among all pSar-lipids, C18-pSar2k and C14-pSar2k have comparable average molecular weight and hydrodynamic diameters with DSPE-PEG2k in aqueous solution with moderate salt content. Therefore, C18-pSar2k was selected for a direct comparison with DSPE-PEG2k as both contain two C18 alkyl chains as anchor (Fig. 2).

The hydrodynamic diameter and ζ potential of liposomes in HEPES buffer were determined by dynamic light scattering (DLS), as shown in Fig. 2, D and SI Table1. All liposomes range 110–130 nm in hydrodynamic diameter with a narrow size distribution (PDI < 0.13), illustrating that the incorporation of pSar-lipid enabled colloidally stable liposomes formation. Either lipid tail length (m = 14, 18) or pSar chain length (M_n = 2 k, 5 k) did not induce any remarkable difference in the size of liposomes. Generally, the surface coating of pSar-lipid or DSPE-PEG2k exhibited an obvious decrease in ζ potential of liposomes due to the surface shielding. A dramatical decrease was found in liposomes when pSar-lipid or PEG-lipid increased from 2.5% to 5.0%, but no further decrease was seen up to 10%, although the surrounding hydrophilic structure may differ at different PEGylation fraction [46]. Exceptionally, around 7 mV of decrease in ζ potential was detected when C14-pSar2k fraction increased from 2.5% (+26.3 mV) to 5.0% (+18.9 mV) and 5.0% to 10% (+11.9 mV). Also, ζ potential reduced from +32.9 mV to +16.9 mV of liposomes when C14-pSar5k fraction increased from 2.5% to 5.0%. In contrast, both pSar-lipid and PEG-lipid that contain two 18-carbon tails did not show any considerable decrease when the molar fraction of lipopolymers in the liposomes varied. As to C18-pSar2k and C18-pSar5k, the surface charge of liposomes was comparable to PEGylated liposomes.

To examine the complexation ability of liposomes, 1.2% agarose gel electrophoresis was used to visualize naked or free mRNA (SI Fig. 2). This result suggests that mRNA was completely bound to cationic liposomes modified with either pSar-lipid or PEG-lipid. Notably, a full complexation of mRNA lipoplexes was observed at N/P 1 and 3 by 2.5% of C14-pSar-lipoplexes and C18-pSar-lipoplexes, respectively, indicating the longer diacyl chains of pSar-lipid partially hampers the interaction between mRNA and cationic liposomes, likely due to a less dynamic nature of lipid nanoparticles. Furthermore, full complexation was observed at N/P 2 for C18-pSar2k-lipoplexes and N/P 3 for PEGylated lipoplexes, which may be due to the increasing content of negatively charged DSPE-PEG2k in the liposomes [47]. FCS measurements employing fluorescently labeled mRNA (Cy5 mRNA) displayed also full complexation in solution. Nevertheless, coating pSar-lipid or DSPE-PEG2k on the surface of cationic liposomes did not dramatically impair their capability to complex mRNA. The formulated mRNA lipoplexes at N/P 5, 10 and 20 were characterized by DLS, as shown in SI Table 2. All mRNA lipoplexes present an average hydrodynamic diameter of approximately 100–250 nm, with ζ potentials ranging from +1 mV to +25 mV. Moreover, all formulations follow the same trend in N/P ratio, a higher N/P ratio, leads to a higher value of the corresponding ζ potential. A typical decrease (up to +16 mV) in ζ potential was obtained when mRNA was complexed by lipoplexes containing an increased molar fraction of C14-pSar regardless of N/P ratio. In contrast, only very slight differences were observed when either C18-pSar5k or DSPE-PEG2k content varied. Interestingly, a comparable ζ potential (around +20 mV) was found from N/P 5 whatever the percentage of C18-pSar2k within formulations, which is probably due to a saturation effect. Overall, all lipoplexes become larger and less positively charged, after mRNA complexation.

4.3. pSar-based lipoplexes displayed promising mRNA transfection efficiency in vitro

To evaluate the influence of pSar-lipid on *in vitro* mRNA delivery performance, fluorescent lipoplexes composed of PE-LR and GFP mRNA at N/P 5, 10 and 20 were applied to adherent Hela cells and suspended Jurkat T cells, respectively. After 24 h' incubation, both cellular uptake and transfection efficiency were quantified by flow cytometry to determine the percentage of transfected cells and mean fluorescence intensity (MFI). The cellular internalization of mRNA lipoplexes was quantified by the signal from PE-LR (Rh, APC-A channel), while mRNA translation was evaluated by GFP expression (GFP, FITC-A channel). Incubating mRNA lipoplexes at N/P 10 with Jurkat T cells and Hela cells for 24 h resulted in over 90% cellular uptake (SI Fig. 3). First, the higher content of shielding lipid in the liposomes, the lower mean fluorescence intensity of Rhodamine (Rh MFI), indicating that incorporation of pSar-lipid or DSPE-PEG2k inhibits the internalization of nanoparticles into Jurkat T cells (SI Fig. 4, A-C). This is in agreement with the previous reports, that the presence of PEG or any other shielding polymer reduced the cellular uptake of lipoplexes and thus decreased the intracellular accumulation and transfection efficiency, due to the inhibition of opsonization (binding between liposomes and proteins), increased surface hydrophilicity and neutralization of the positive surface charge required for binding to the negatively charged cell surface [48,49]. Second, as the length of pSar chain increased from 2 k to 5 k, the Rh MFI was decreased with it, especially for C18-pSar2k and C18-pSar5k. As well, the anchor chain length of pSar-lipid also influenced the cellular uptake. For example, a much higher Rh MFI was observed in the cells treated with C14-pSar5k-containing mRNA lipoplexes than that of analogues containing C18-pSar5k, regardless of their molar contents (SI Fig. 4 A2, B2, C2). Taken together, our findings underline that both the molar fraction of pSar-lipids, length of the pSar chain and diacyl chain are of major importance for cellular uptake, which is in line with PEG-lipids. In a direct comparison to DSPE-PEG2k, C18-pSar2k resulted in a remarkably higher Rh MFI compared to the analogues of PEGylated lipoplexes in both Jurkat T cells (SI Fig. 4, A3, B3, C3) and Hela cells (SI Fig. 4, D3, E3, F3).

Modification of the liposome surface with shielding material compromised cellular uptake, which was well demonstrated in Jurkat T cells but much less notable in Hela cells. As reported, the liposome adsorption or uptake into tumor cells was caused by re-uptake of PEG-lipid on the liposomal membrane. The high residual PEG-lipid on the liposomes' membrane enabled a stable modification of liposomes and thus promoted liposome uptake. A shorter diacyl chain length (DPG-PEG2k) led to a higher cellular uptake than that of DSG-PEG2k, which was in agree with our findings and relates to a reduced shielding of cationic charges caused by reduced integration and stability of C14-lipopolymers in the lipoplexes structure [51].

The role of pSar-lipid or PEG-lipid on transfection efficiency was also explored, by exposing cells to mRNA (encoding for GFP) lipoplexes at N/P 5, 10 and 20, for 24 h to allow for protein expression (Fig. 3, SI Fig. 5). Clearly, the higher molar fraction of pSar-lipid or DSPE-PEG2k in the formulations, the lower GFP expression in Jurkat T cells and Hela cells (Fig. 3). In Jurkat T cells, the low GFP expression is highly likely due to the less efficient cellular uptake (SI Fig. 4, B). The highest percentage of GFP -expressing cells was approximately 40%, which was observed in cells exposed to 2.5% C18-pSar2k-containing lipoplexes. When the content of C18-pSar2k increased to 5% and 10%, the transfection efficiency dramatically decreased to 20% and 5%, respectively. In Hela

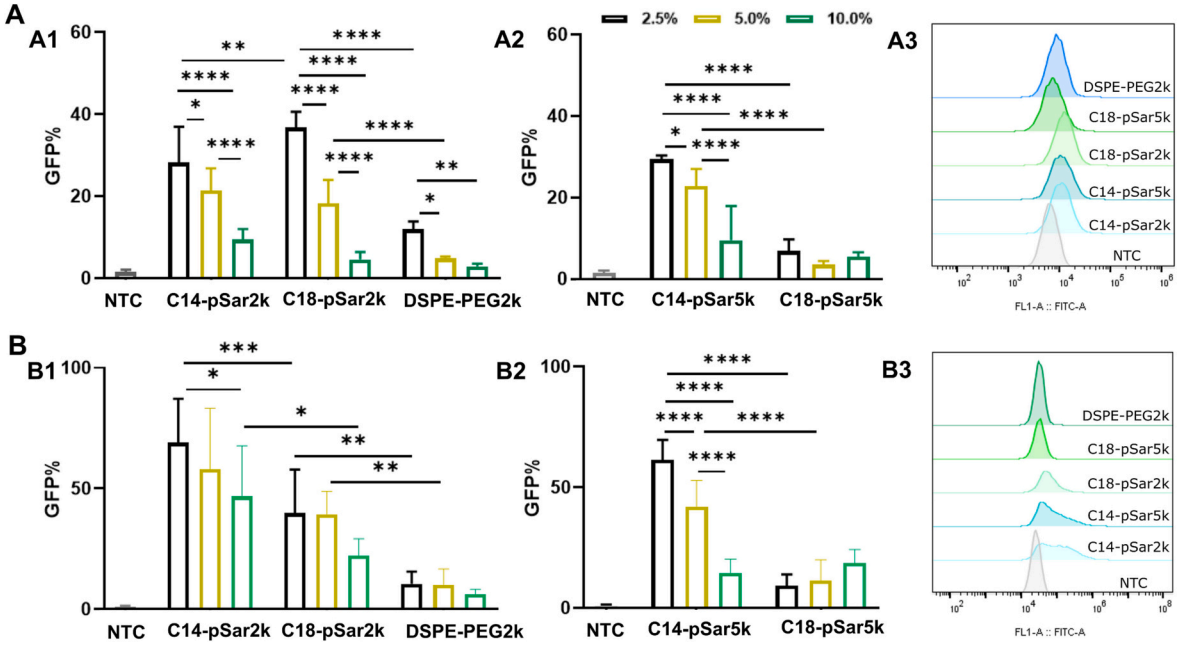

Fig. 3. Lipoplexes containing GFP mRNA and PE-LR labeled liposomes were incubated with (A) Jurkat T cells and (B) Hela cells for 24 h to examine transfection efficiency. Lipoplexes were prepared by incubating equal volume of mRNA and liposomes at N/P 10. At the end of incubation, cells were harvested and quantified by flow cytometry, as demonstrated in (A1, A2) of Jurkat T cells and (B1, B2) Hela cells. Representative images of (A3) Jurkat T cells and (B3) Hela cells, after transected with mRNA lipoplexes composed of 2.5% DSPE-PEG2k or pSar-lipid-polyplexes. All the data was averaged from three independent experiments ($n = 9$).

cells, 2.5% C14-pSar2k-modified mRNA lipoplexes led the highest protein expression (GFP-positive cells 70%), and the transfection efficiency also decreased when the molar fraction of pSar-lipid increased. The observation that an increasing PEG percentage induced a reduction of transfection efficiency was also found in mRNA PEGylated LNPs, where 0.5% DMG-PEG2k LNPs elicited the highest luciferase expression in mice after subretinal injections, which was 2-, 5- and 19-fold than LNPs containing 1.5%, 3.0% and 5.0% DMG-PEG2k, respectively [52]. Not only the percentage of shielding lipid but also the pSar chain length affected the mRNA translation. This is most obvious in the lipoplexes containing 2.5% C18-pSar-lipid, where the transfection efficiency was strongly decreased from 37% to 7% in Jurkat T cells when pSar chain increased from 2 k to 5 k.

Next, we studied the influence of anchor chains of pSar-lipid on their transfection efficiencies. In Jurkat T cells, replacing C18 with C14 of pSar5k-lipids as alkyl anchor led to a decrease (up to 20%) in transfection efficiency (Fig. 3, A). A similar phenomenon occurred in Hela cells, with 20–30% decrease in GFP-positive cells transfected with mRNA lipoplexes containing C18-pSar2k than that of C14-pSar2k. When M_n of the pSar chain increased to 5 k, the reduction of GFP-positive cells (%) was more significant with a shorter alkyl lipid, decreasing from 60%, 40% for 2.5% and 5.0% C14-pSar5k, to 10% for 2.5% and 5.0% C18-pSar5k, respectively. Based on those findings we could conclude that C14-pSar-lipids yielded higher transfection efficiencies compared to the analogues of C18-pSar-lipids in these two cell lines, while stability in buffer remained on the same level. This is in agreement with the findings for PEGylated lipid formulations. Hattori et al. reported the major role of anchor of PEG derivate in gene silencing by siRNA lipoplexes. Compared to short bisalkyl chains (C14), long bisalkyl chains (C16-C18) PEG-lipids tended to inhibit the gene silencing effects in cells, which may be due to the less efficient detachment of PEG-lipids from lipoplexes in culture medium. Additionally, they predicted the electrostatic interactions between the phosphate groups of DSPE-PEG2k and amine group of cationic lipids may also inhibit the detachment of PEG-lipid from lipoplexes, thus contributed to the reduced gene silencing [47]. To sum up, these tests demonstrate that pSar-lipid (except C18-pSar5k) outperformed in delivering mRNA into adherent cells and suspension cells, compared to DSPE-PEG2k. The fraction of pSar-lipid, alkyl chain length and pSar chain length did affect the cellular uptake and protein expression of mRNA lipoplexes. Lipoplexes containing C14-pSar2k, C18-pSar2k and C14-pSar5k at 2.5% and 5.0% yielded a higher transgene expression than other formulations in both cell lines and were further explored *in vivo*.

4.4. *pSar-liposomes exhibited comparable circulation behavior with PEGylated liposomes in vivo*

Zebrafish embryos have been validated as an attractive screening tool to predict the fate of nanoparticles, in which the fluorescent nanoparticles can be visualized at both the whole animal and individual cells (*e.g.*, macrophages, endothelial cells) by confocal fluorescence microscope in the optical transparent larvae [53,54]. To evaluate the influence of pSar-lipopolymers on properties of liposomes, the fluorescently labeled liposomes were intravenously injected (*i.v.*) into 2.5 dpf (days-post fertilization) zebrafish embryos. A mutant zebrafish strain, Tg(*kdrl*: GFP) embryos, with stable GFP expression in blood vessels (endothelial cells), was employed to visualize the liposome-EC interactions and to exclude acute toxicity effects related to the employed formulations. As we found in previous study, cationic liposomes were associated with ECs and cleared from the circulation within 1 h after systemic injection [55]. When liposomes are PEGylated, the interaction between liposomes and ECs is expected to be limited, thus allowing for a prolonged circulation in the blood stream [55]. Therefore, the number of liposomes in circulation could reflect the shielding effect of PEG-lipid or pSar-lipid to some extent. Fig. 4, A shows an example of freely circulating liposomes in a zebrafish embryo. From the whole embryos view, the liposomes (magenta) circulated in the lumen of blood vessels (green), and mostly accumulated into the common cardia vein (CCV) and posterior cardinal vein (PCV). A closer look at the biodistribution of liposomes and the vascular classification at the tissue level are displayed in the caudal area, where most of liposomes were found in the dorsal aorta (DA), caudal hematopoietic tissue (CHT) and caudal veins (CV).

First, we checked the biodistribution of PEGylated liposomes at

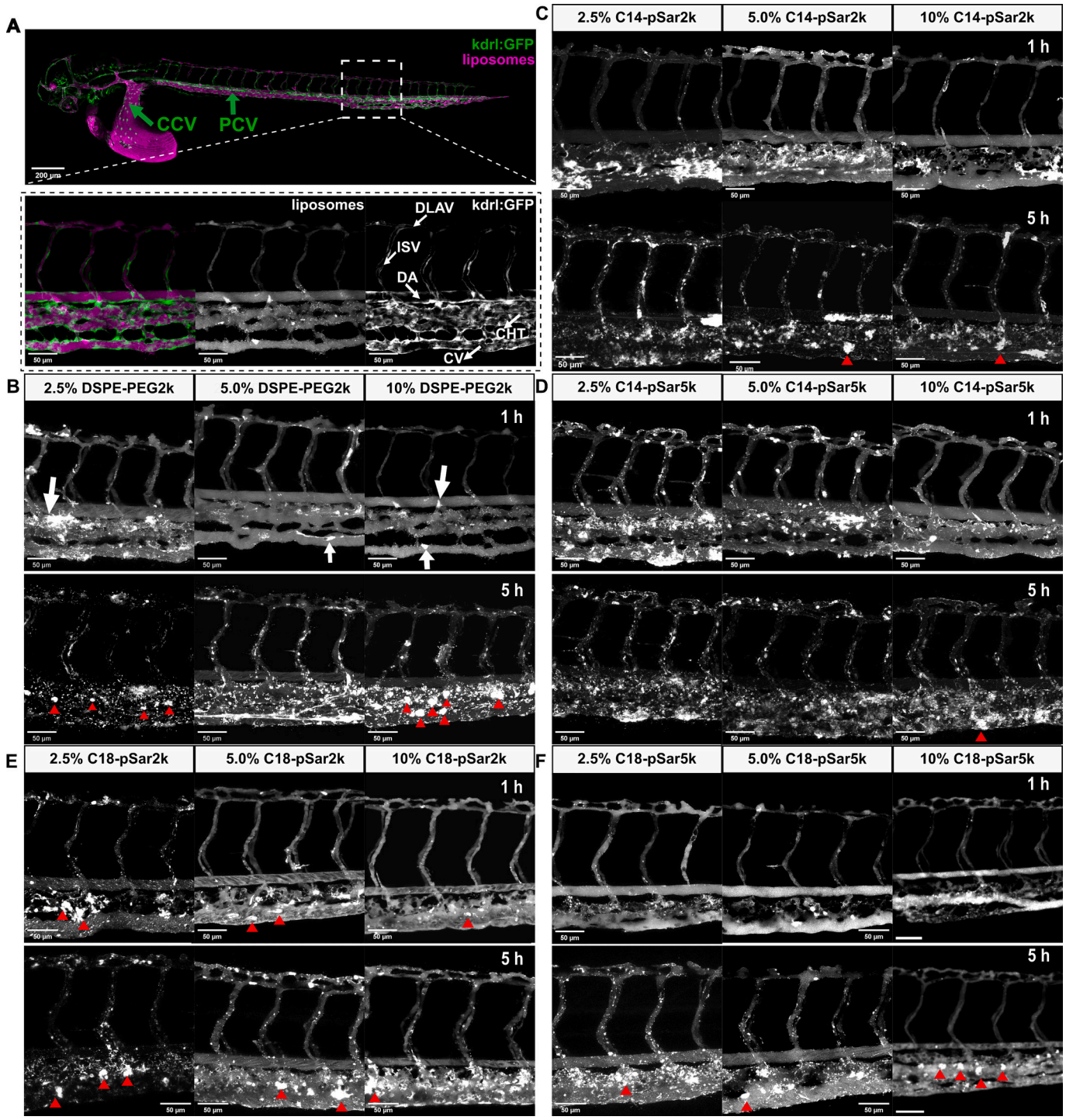

Fig. 4. Biodistribution of liposomes (1 nL, 30 mM) modified with (B) DSPE-PEG2k, (C) C14-pSar2k, (D) C14-pSar5k, (E) C18-pSar2k and (F) C18-pSar5k after intravenous injection into 2.5 dpf zebrafish embryos. (A) Representative images of whole embryo view at 1 h after administration with 10% PEGylated liposomes. Tg (*Kdrl*:GFP) zebrafish embryos expressed GFP (green) within all endothelial cells (ECs). Common cardinal vein (CCV) and posterior cardinal vein (PCV) are the two main venous vessels, as green arrows indicate. Different blood vessels were indicated by white arrows: dorsal aorta (DA), caudal hematopoietic tissue (CHT), caudal vein (CV), intersegmental vessel (ISV), dorsal longitudinal anastomotic vessel (DLAV). PE-LR labeled liposomes were shown in magenta. Tissue level views (40× lens, magnification of the white square) displayed the merged image of liposomes (magenta) and ECs (green) and separated images in gray. (B—F) Representative biodistribution images of (B) 2.5%, 5.0% and 10% PEGylated liposomes (C) C14-pSar2k-, (D) C14-pSar5k-, (E) C18-pSar2k- and (F) C18-pSar5k-coated liposomes in 2.5 dpf zebrafish embryos at 1 hpi and 5 hpi. White arrows show liposome aggregates at 1 hpi, and red triangles show that the liposomes were internalized into macrophages. Scale bar: 200 μm for whole embryo view and 50 μm for tissue level view. (For interpretation of the references to colour in this figure legend, the reader is referred to the web version of this article.)

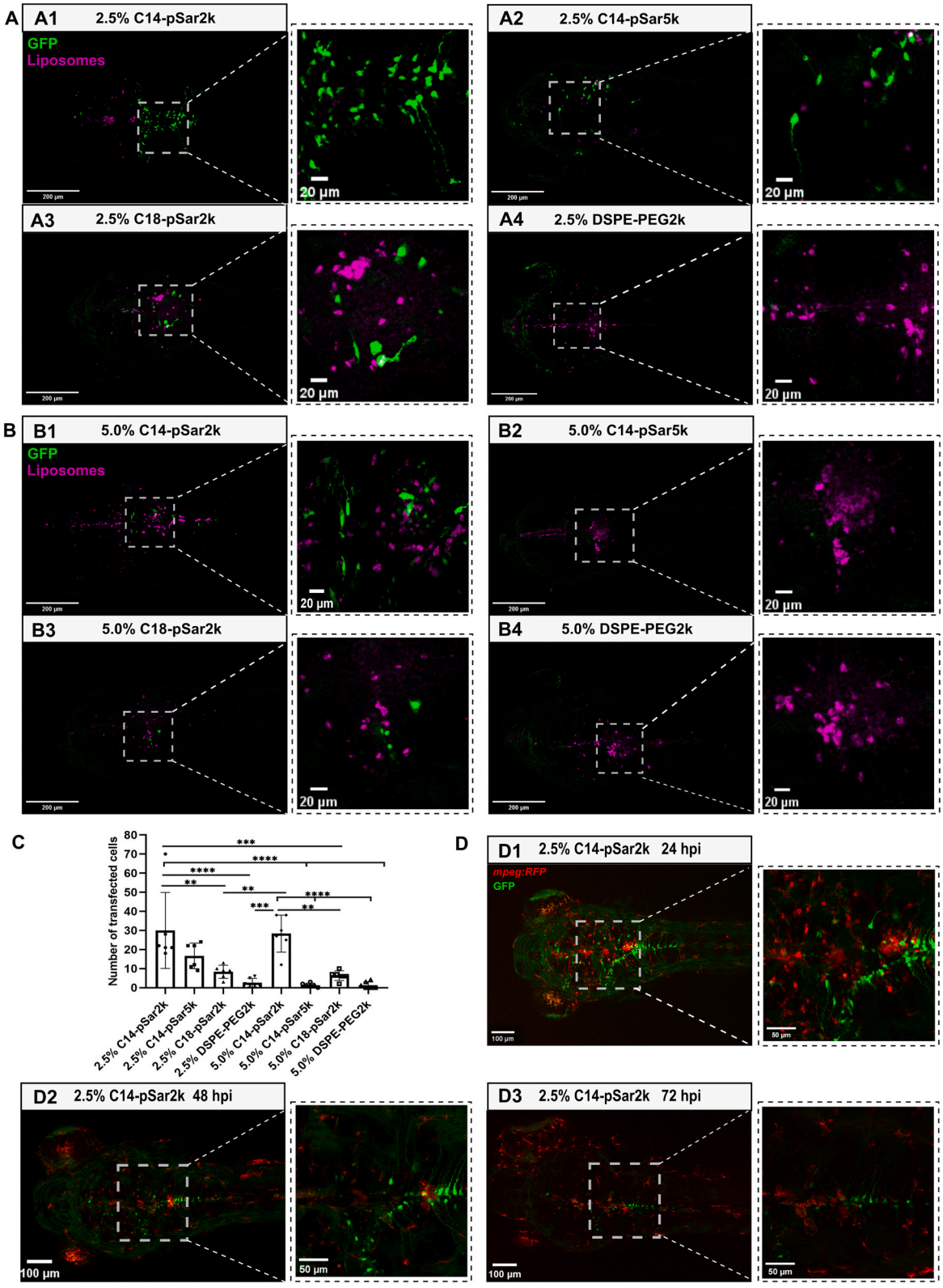

Fig. 5. GFP expression within 2.5 dpf zebrafish embryos at 24 hpi in the dorsal view. 1.5 nL lipoplexes (DOTAP/DOPE/DSPE-Rhodamine B/pSar-lipid or DSPE-PEG2k, 30 mM, N/P 10) containing GFP mRNA (100 ng/μL) were injected into the zebrafish brain. (A-C) GFP (green) expression in wildtype ABTL zebrafish embryos that were injected with (A1-A4) 2.5% C14-pSar2k, C14-pSar5k, C18-pSar2k and DSPE-PEG2k lipoplexes (magenta) and (B1-B4) 5.0% C14-pSar2k, C14-pSar5k, C18-pSar2k and DSPE-PEG2k lipoplexes in dorsal view (scale bar: 200 μm). (C) Quantification of GFP-expressing cells in the brain of zebrafish embryos after intracranial injection ($n = 6$). (D) GFP (green) expression within 2.5 dpf Tg(mpeg1: RFP) zebrafish embryos (macrophages in magenta) at (D1) 24 hpi, (D2) 48 hpi and (D3) 72 hpi in the dorsal view of brain (scale bar: 200 μm, 100 μm, 50 μm). (For interpretation of the references to colour in this figure legend, the reader is referred to the web version of this article.)

various time points after systemic injection (Fig. 4, B). Within first 1 h, 2.5% PEGylated liposomes tended to aggregate (as white arrow indicates) and started to associate with all ECs (especially ECs in CHT), which was not observed in liposomes containing 5.0% and 10% DSPE-PEG2k. At 5 hpi, 2.5% PEGylated liposomes were mostly cleared from the circulation by scavenger endothelial cells (SECs) and macrophages, and most of PEGylated liposomes with higher content of DSPE-PEG2k (5.0%, 10%) were still in circulation despite their accumulation in ECs as well. After 1 day, all PEGylated liposomes were associated with SECs, and no obvious liposomes-associated fluorescence was found in circulation (SI Fig. 6, A). These findings, therefore, confirm that PEGylation can improve the circulation time and stability of liposomes due to the shielding effect, which is more notable in the liposomes containing a higher content of DSPE-PEG2k. The cellular internalization of PEGylated liposomes into macrophages was observed after 5 hpi, which was indicated by red arrows.

Then, we injected liposomes containing pSar-lipid into 2.5 dpf zebrafish embryos as well (Fig. 4, C—F). At 1 hpi, all pSar-coating liposomes were in circulation, but the amounts of liposomes in the vasculature varied. The C14-pSar-containing liposomes started to associate with ECs. The higher content of C14-pSar in formulation, the more liposomes remained circulating. The content of C18-pSar2k also affected the amount of liposomes circulating *in vivo*, while the content of C18-pSar5k showed a rather limited influence on this, which probably due to the 2.5% of C18-pSar5k already exhibited a sufficient shielding effect on liposomes. In addition, sarcosine repeat units and alkyl chain lengths of pSar-lipids also have impact on the liposome circulation. For example, when the M_n of pSar was extended from 2 k to 5 k, a higher amount of pSar-5 k-containing liposomes were in circulation even at a lower content of 2.5%. Interestingly, we found that 2.5% C18-pSar5k-liposomes were completely in circulation without any interacting with ECs, while 2.5% C14-pSar5k-liposomes were found to be associated with ECs, which reflects the reduced stability of C14-lipid-liposomes than the analogues of C18-lipid-liposomes. At 5 hpi, all C14-pSar-modified liposomes were cleared from circulation and accumulated within ECs (Fig. 4, C), while most C18-pSar-containing liposomes were hardly associated with ECs and freely circulating. But 2.5% C18-pSar2k-liposomes showed association with ECs (Fig. 4, E). This finding again suggests that C14-pSar was less stable integrated in the liposomes and thus is less efficient in shielding the cationic liposomes core [47]. After 24 hpi, all liposomes were eventually removed from circulation and taken up by ECs and macrophages (SI Fig. 6). In addition, any acute toxicity related to the application of liposomes was not observed.

To sum up, coating with pSar-lipid improved the circulation of cationic liposomes in zebrafish embryos in a dose-dependent manner and did not cause any detectable acute toxicity. Both content of pSar-lipid, pSar average molecular weight and alkyl chain length affect the circulation and biodistribution of liposomes. The longer pSar chain length or longer alkyl chain length or both promoted the circulation time of pSar-incorporated liposomes. The shielding effect of pSar-lipid and DSPE-PEG2k on liposomes follows C18-pSar5k > DSPE-PEG2k ~ C18-pSar2k > C14-pSar5k > C14-pSar2k.

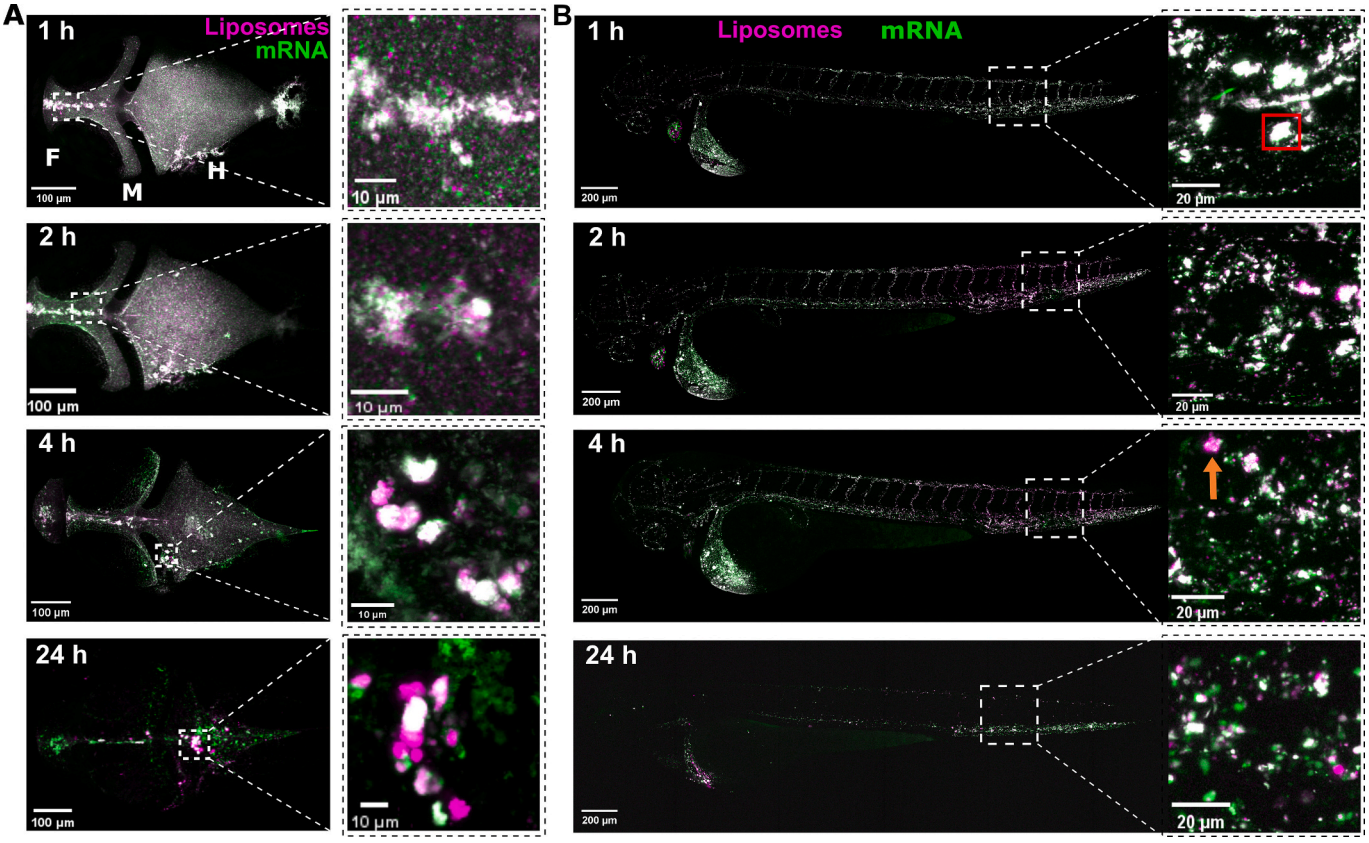

Fig. 6. Biodistribution of lipoplexes composed of fluorescently labeled liposomes (megenta, DOTAP/DOPE/DSPE-Rhodamine /C14-pSar2k at a molar ratio of 48.65/48.65/0.2/2.5, 30 mM) and Atto488 labeled luciferase mRNA (green, 150 pg mRNA, N/P 10) (A) in brain after intraventricular injection and (B) in whole embryo after intravenous injection in 2.5 dpf ABTL zebrafish embryos. Confocal images were taken by 10× lens for whole embryos view (scale bar: 100 μm) and 40× lens (scale bar: 20 μm) at 1 hpi, 2 hpi, 4 hpi and 24 hpi. Co-localized liposomes and mRNA were shown in red square. Free liposomes were marked by orange arrows in the zoomed images, respectively. F: forebrain; M: midbrain; H: hindbrain. (For interpretation of the references to colour in this figure legend, the reader is referred to the web version of this article.)

4.5. pSar-modified lipoplexes resulted in more efficient translation after intracranial injection

It has been reported that cationic lipid can help liposomes to across BBB by increasing the permeability of anionic EC junctions [62]. Based on the *in vitro* transfection efficacy, we further verified whether these findings could be translated into *in vivo* applications or not. First, we explored the transfection efficiency of mRNA lipoplexes in 2.5 dpf zebrafish embryos through systemic administration of the two most promising formulations composed of 2.5% and 5% C14-pSar2k. As displayed in SI Fig. 7, mRNA lipoplexes were mainly taken up by scavenger endothelial cells and macrophages at 24 hpi and resulted in an intense GFP fluorescence in individual endothelial cells. However, cell specific transfection can only be achieved in ECs for those tested formulations, and we did not detect any transfection in the CNS of zebrafish. At present, there are very limited nanoparticles suitable for intracerebral mRNA delivery. Although nanoparticles can assist mRNA crossing the BBB by systemic injection, their drawbacks, such as less accumulation and toxicity in the brain, remains a challenge [5]. To achieve specific mRNA transfer to the CNS, local injection seems favorable. Local administration exhibits several advantages including lower therapeutic dose and less side effects have gained attention. Here, we selected the mRNA formulations with higher *in vitro* transfection efficiency (Fig. 3) for intracerebral injection of zebrafish embryos. Lipoplexes containing GFP mRNA (1.5 nL, 150 pg) were injected into the hindbrain ventricle of 2.5 dpf zebrafish embryos. At 24 hpi, six fish were randomly selected in each group for visualization and quantification of GFP expression.

The representative confocal images show that lipoplexes can be traced by lipid associated fluorescence (magenta) as well as GFP (green) expression in the brain of zebrafish embryos (Fig. 5). All lipoplexes remained in brain at 24 hpi, and there was no detectable difference in the biodistribution of the different lipoplexes in the zebrafish brain (Fig. 5, A & B). In general, an overall amount of 2.5% shielding lipid resulted in a more efficient mRNA translation than that in the case of lipoplexes with 5.0% pSar-lipids. For example, increasing the molar fraction of C14-pSar5k from 2.5% to 5.0% led to a considerable reduction in GFP expression. The GFP signal was even close to the autofluorescence from pigment cells in the eyes and skin, when mRNA lipoplexes containing 5.0% PEGylated lipids were injected into zebrafish embryos. Notably, no dramatical decrease of GFP-positive cells was found in the case of C14-pSar2k- or C18-pSar2k-containing lipoplexes by varying the pSar-lipid content. To verify our hypothesis that limited co-localization of GFP and liposomes was due to the degradation of liposomes, we intracranially injected 2.5% C14-pSar2k-containing GFP-encoding mRNA lipoplexes in 2.5 dpf zebrafish and visualized the GFP expression and its co-localization with liposomes at 8 hpi. As shown in SI Fig. 9, we clearly saw the GFP expression and more GFP+/liposomes double-positive cells (a, b, c). When we took a closer look at the double-positive cells, the GFP signal was rather low, while liposomes were not visible when GFP expression was evidenced. This may suggest that it is pre-requisite to degrading liposomes or unpacking mRNA for GFP-encoded mRNA translation. Overall, 2.5% and 5.0% C14-pSar2k-containing mRNA lipoplexes showed the most robust and pronounced GFP expression.

To better evaluate the transfection efficiency, we quantified the number of GFP-expressing cells in six embryos per group (SI Fig. 8), and the higher number of transfected cells indicates the better transfection efficiency. As Fig. 5, D displays, a significantly higher number of GFP-positive cells was observed in the zebrafish embryos that were injected with 2.5% C14-pSar2k-lipoplexes (average number of GFP-positive cells: 30 ± 20). Extending the sarcosine chain length to 5 k, however, lowered the GFP expression significantly. Also the longer alkyl chain length of C18 led to a drastically reduced GFP production, again implying that the shorter alkyl chain length facilitated transfection of mRNA lipoplexes. In comparison, lipoplexes with 2.5% PEGylated lipids led to a relatively limited protein expression (average number of GFP-positive cells: 3 ± 2). These results were consistent with *in vitro* findings, both which indicate that the chain length of pSar and alkyl group as well as the content of shielding lipids impact mRNA translation.

Lastly, we investigated the type of cells being primarily transfected, which are microglia or neurons in our case (Fig. 5, A & B). Microglia are part of the resident macrophages, and these specialized phagocytes play an essential role in the vertebrate central nervous system by engulfing damaged neurons and foreign particles [56]. To precisely specify the cell type that were successfully transfected in the brain of zebrafish embryos after intracranial injection, Tg(*mpeg1*: RFP), a mutant zebrafish line with macrophages that stably express red fluorescent protein (RFP), was used for the application of the most promising formulation of 2.5% C14-pSar2k-containing mRNA lipoplexes. We observed the GFP signal in zebrafish brain for 72 hpi, and it decreased over time (Fig. 5, D). Interestingly, we did not find any co-localization of GFP (green) and macrophages (red) in zebrafish brain, indicating the GFP-expressing cells are highly likely not microglia. Typically, a neuron is composed of a cell body, an axon and dendrites. Moreover, descending neurons are symmetrically distributed in the hindbrain of zebrafish embryos [57,58]. Given that those GFP-positive cells have a long tail (around hundred nanometer, also similar in shape to an axon) and localize in the ventricle of hindbrain, we assumed they may be neurons [59–61]. In conclude, C14-pSar2k at lower content lipopolymer contents (2.5%, 5.0%) were most effective in the transfection of neurons and lead to the most stable mRNA induced GFP expression in the CNS. Interestingly, we did not observe any signs for lipoplexes related toxicity in any of the zebrafish larvae.

4.6. pSar-lipoplexes can release mRNA in zebrafish embryos

To track mRNA lipoplexes and study mRNA release *in vivo*, lipoplexes composed of DOTAP, DOPE, C14-pSar2k and PE-LR (molar ratio of 48.65/48.65/2.5/0.2) were used to complex Atto488 labeled luciferase mRNA into lipoplexes and subsequently administrated into zebrafish embryos through either intraventricular injection or intravenous injection. The colocalization (white) of liposomes (magenta) and mRNA (green) reflects the stability of mRNA lipoplexes in some extent, where the less colocalization indicates more mRNA release. Note that some absence of co-localization of liposomes and mRNA might be attributed to the technical limitations, as confocal microscopy subsequently scanned liposomes and mRNA, while the lipoplexes kept circulating during the switch of laser channels.

As displayed in Fig. 6, co-localization of mRNA and DSPE-Rhodamine B was found in the zebrafish embryos after both local and systemic administration at 1 hpi, illustrating a stable encapsulation of mRNA in the lipoplexes within first 1 h. Due to the injected fluorescent lipoplexes in the ventricles, the ventricles in the forebrain, heart and hindbrain could be clearly observed, confirming the intraventricular injection were successful (Fig. 6, A). At 2 hpi co-localization was decayed and separated mRNA and lipid associated fluorescence became visible, which indicated that mRNA started to be released from the lipoplexes and translocated to other subcellular compartments. After systemic injection, the red fluorescence signal increased over time especially in the tail regions through the whole embryo view, which may be due to the partial mRNA release or degradation (Fig. 6, B). After 24 h, the fluorescent lipids and mRNA were clearly separated and only a few areas with co-location of lipids and mRNA were found in the hindbrain ventricle (Fig. 6, A) and endothelial cells (ECs) (Fig. 6, B), suggesting a full mRNA release and lipoplexes disintegration within 24 h. These findings may explain a very limited colocalization of GFP (green) and liposomes (magenta) found in the transfection studies (Fig. 5). Importantly, all injected embryos were alive without any abnormal appearance and movement change after intravenous or intracerebral injection over the time frame of the experiment of 3 days, demonstrating the injected lipoplexes were safe and do not case acute toxic effects.

5. Conclusion

The development of lipid formulation for mRNA delivery has gained considerable interest for neurological diseases, and PEG has become a key component for improving stability and circulation time of mRNA lipid formulations. However, the ABC phenomenon and the immune responses towards PEGylated formulation, highlight an urgent demand to develop safe and efficient PEG-free delivery systems. In this work, we developed the PEG-free lipid formulation to intracerebrally deliver mRNA. Firstly, we synthesized four pSar-lipids with defined lipophilic anchor and hydrophilic chain length. We could confirm that the pSar can substitute DSPE-PEG2k in cationic lipid formulations, by studying the circulation of modified liposomes in zebrafish embryos after systemic administration. We found that either a longer hydrophilic chain and/or lipophilic anchor of pSar-lipids or a higher content of pSar-lipid in formulations contributed to the prolonged circulation and reduced transfection efficiency of lipid formulations *in vitro* and *in vivo*. 2.5% C14-pSar2k-containing mRNA lipoplexes showed the most robust protein expression, while C18-pSar5k-lipoplexes exhibited a longer circulation half-life. Therefore, a critical balance between circulation half-life and transfection efficiency is highly suggested to be maintained to develop more effective pSar-modified lipid formulations, based on the desired goal in the treatments. We also found a good correlation between *in vitro* and *in vivo* studies, suggesting zebrafish embryos as a powerful tool to screen liposomal formulations. Finally, we showed the efficacy of pSar in mRNA lipid formulations for local administration in the CNS. Compared to DSPE-PEG2k modified lipoplexes, an improved transgene expression in brain cells without any acute toxicity was observed. A detailed understanding of the pSar-lipids control over liposomal properties and fine-tuning of anchor lipid and pSar chain length beyond the molar fraction in those formulations, will enable the therapeutic use of mRNA lipid formulations even for local applications in the CNS, which could be beneficial in the clinical translations of mRNA-based therapies for CNS disorders.

CRediT authorship contribution statement

Dongdong Bi: Conceptualization, Methodology, Investigation, Data curation, Writing – original draft, Visualization. **Dennis Mark Unthan:** Methodology, Investigation, Writing – original draft. **Lili Hu:** Investigation. **Jeroen Bussmann:** Methodology, Writing – review & editing, Supervision. **Katrien Remaut:** Writing – review & editing. **Matthias Barz:** Conceptualization, Writing – review & editing, Supervision, Project administration, Funding acquisition. **Heyang Zhang:** Conceptualization, Methodology, Investigation, Writing – original draft, Writing – review & editing, Supervision.

Declaration of Competing Interest

M.B. is co-inventor of PCT WO2020069718A1: RNA particles comprising polysarcosine. All other authors declare the absence of any conflict of interest.

Data availability

Data will be made available on request.

Acknowledgement

D.B. would like to acknowledge the financial support from China Scholarship Council (No. 201906210053). M. B. acknowledges support by the CRC1066-2/-3 (Project B12) for the development of polysarcosine lipids and formulations thereof.

Appendix A. Supplementary data

Supplementary data to this article can be found online at https://doi.org/10.1016/j.jconrel.2023.02.021.

References

[1] G.N. Collaborators, Global, regional, and national burden of neurological disorders, 1990–2016: a systematic analysis for the Global Burden of Disease Study 2016, Lancet Neurol. 18 (2019) 459–480.
[2] X. Hou, T. Zaks, R. Langer, Y. Dong, Lipid nanoparticles for mRNA delivery, Nat. Rev. Mater. 6 (2021) 1078–1094.
[3] K. Anthony, RNA-based therapeutics for neurological diseases, RNA Biol. 19 (2022) 176–190.
[4] Y. Fukushima, S. Uchida, H. Imai, H. Nakatomi, K. Kataoka, N. Saito, K. Itaka, Treatment of ischemic neuronal death by introducing brain-derived neurotrophic factor mRNA using polyplex nanomicelle, Biomaterials 270 (2021), 120681.
[5] H. Peng, X. Guo, J. He, C. Duan, M. Yang, X. Zhang, L. Zhang, R. Fu, B. Wang, D. Wang, H. Chen, M. Xie, P. Feng, L. Dai, X. Tang, J. Luo, Intracranial delivery of synthetic mRNA to suppress glioblastoma, Mol. Ther. Oncoly. 24 (2022) 160–170.
[6] R. Nieto Montesinos, Liposomal Drug Delivery to the Central Nervous System, 2017, pp. 213–241.
[7] J. Rip, Liposome technologies and drug delivery to the CNS, Drug Discov. Today Technol. 20 (2016) 53–58.
[8] B.S. Pattni, V.V. Chupin, V.P. Torchilin, New developments in liposomal drug delivery, Chem. Rev. 115 (2015) 10938–10966.
[9] K. Ogawa, N. Kato, S. Kawakami, Recent strategies for targeted brain drug delivery, Chem. Pharm. Bull. 68 (2020) 567–582.
[10] C. Duma, O. Kopyov, A. Kopyov, M. Berman, E. Lander, M. Elam, M. Arata, D. Weiland, R. Cannell, C. Caraway, S. Berman, K. Scord, L. Stemler, K. Chung, S. Khoudari, R. McRory, C. Duma, S. Farmer, A. Bravo, C. Yassa, A. Sanathara, E. Singh, B. Rapaport, Human intracerebroventricular (ICV) injection of autologous, non-engineered, adipose-derived stromal vascular fraction (ADSVF) for neurodegenerative disorders: results of a 3-year phase 1 study of 113 injections in 31 patients, Mol. Biol. Rep. 46 (2019) 5257–5272.
[11] T.T.H. Thi, E.J.A. Suys, J.S. Lee, D.H. Nguyen, K.D. Park, N.P. Truong, Lipid-based nanoparticles in the clinic and clinical trials: from cancer nanomedicine to COVID-19 vaccines, Vaccines (Basel) 9 (2021).
[12] X. Liu, I. Tang, Z.A. Wainberg, H. Meng, Safety considerations of cancer nanomedicine-a key step toward translation, Small (Weinheim an der Bergstrasse, Germany) 16 (2020) e2000673.
[13] A. Soundararajan, A. Bao, W.T. Phillips, R. Perez 3rd, B.A. Goins, [(186)Re] Liposomal doxorubicin (Doxil): in vitro stability, pharmacokinetics, imaging and biodistribution in a head and neck squamous cell carcinoma xenograft model, Nucl. Med. Biol. 36 (2009) 515–524.
[14] R. Tenchov, R. Bird, A.E. Curtze, Q. Zhou, Lipid Nanoparticles—From Liposomes to mRNA vaccine delivery, a landscape of research diversity and advancement, ACS Nano 15 (2021) 16982–17015.
[15] K. Shiraishi, M. Yokoyama, Toxicity and immunogenicity concerns related to PEGylated-micelle carrier systems: a review, Sci. Technol. Adv. Mater. 20 (2019) 324–336.
[16] J. Vrieze, Suspicions grow that nanoparticles in Pfizer's COVID-19 vaccine trigger rare allergic reactions, Science (2020), https://doi.org/10.1126/science.abg2359.
[17] Y. Mima, Y. Hashimoto, T. Shimizu, H. Kiwada, T. Ishida, Anti-PEG IgM is a major contributor to the accelerated blood clearance of polyethylene glycol-conjugated protein, Mol. Pharm. 12 (2015) 2429–2435.
[18] M. Estapé Senti, C.A. de Jongh, K. Dijkxhoorn, J.J.F. Verhoef, J. Szebeni, G. Storm, C.E. Hack, R.M. Schiffelers, M.H. Fens, P. Boross, Anti-PEG antibodies compromise the integrity of PEGylated lipid-based nanoparticles via complement, J. Control. Release 341 (2022) 475–486.
[19] L. Shi, J. Zhang, M. Zhao, S. Tang, X. Cheng, W. Zhang, W. Li, X. Liu, H. Peng, Q. Wang, Effects of polyethylene glycol on the surface of nanoparticles for targeted drug delivery, Nanoscale 13 (2021) 10748–10764.
[20] T. Ishida, M. Harada, X.Y. Wang, M. Ichihara, K. Irimura, H. Kiwada, Accelerated blood clearance of PEGylated liposomes following preceding liposome injection: effects of lipid dose and PEG surface-density and chain length of the first-dose liposomes, J. Control. Release 105 (2005) 305–317.
[21] B.-M. Chen, T.-L. Cheng, S.R. Roffler, Polyethylene glycol immunogenicity: theoretical, clinical, and practical aspects of anti-polyethylene glycol antibodies, ACS Nano 15 (2021) 14022–14048.
[22] X. Zhu, W. Tao, D. Liu, J. Wu, Z. Guo, X. Ji, Z. Bharwani, L. Zhao, X. Zhao, O. C. Farokhzad, J. Shi, Surface De-PEGylation controls nanoparticle-mediated siRNA delivery in vitro and in vivo, Theranostics 7 (2017) 1990–2002.
[23] A.S. Abu Lila, K. Nawata, T. Shimizu, T. Ishida, H. Kiwada, Use of polyglycerol (PG), instead of polyethylene glycol (PEG), prevents induction of the accelerated blood clearance phenomenon against long-circulating liposomes upon repeated administration, Int. J. Pharm. 456 (2013) 235–242.
[24] Y. Wu, Y. Li, G. Lv, W. Bu, Redox dyshomeostasis strategy for tumor therapy based on nanomaterials chemistry, Chem. Sci. 13 (2022) 2202–2217.
[25] P.H. Kierstead, H. Okochi, V.J. Venditto, T.C. Chuong, S. Kivimae, J.M.J. Fréchet, F.C. Szoka, The effect of polymer backbone chemistry on the induction of the accelerated blood clearance in polymer modified liposomes, J. Control. Release 213 (2015) 1–9.

[26] A. Birke, J. Ling, M. Barz, Polysarcosine-containing Copolymers: Synthesis, Characterization, Self-assembly, and Applications, Progr. Polym. Sci. 81 (2018) 163–208.
[27] I. Negwer, A. Best, M. Schinnerer, O. Schäfer, L. Capeloa, M. Wagner, M. Schmidt, V. Mailänder, M. Helm, M. Barz, H.-J. Butt, K. Koynov, Monitoring drug nanocarriers in human blood by near-infrared fluorescence correlation spectroscopy, Nat. Commun. 9 (2018) 5306.
[28] B. Weber, A. Birke, K. Fischer, M. Schmidt, M. Barz, Solution properties of polysarcosine: from absolute and relative molar mass determinations to complement activation, Macromolecules 51 (2018) 2653–2661.
[29] F. Fenaroli, U. Repnik, Y. Xu, K. Johann, S. Van Herck, P. Dey, F.M. Skjeldal, D. M. Frei, S. Bagherifam, A. Kocere, R. Haag, B.G. De Geest, M. Barz, D.G. Russell, G. Griffiths, Enhanced permeability and retention-like extravasation of nanoparticles from the vasculature into tuberculosis granulomas in zebrafish and mouse models, ACS Nano 12 (2018) 8646–8661.
[30] P.H. Maurer, D. Subrahmanyam, E. Katchalski, E.R. Blout, Antigenicity of polypeptides (Poly Alpha Amino Acids), J. Immunol. 83 (1959) 193.
[31] S.S. Nogueira, A. Schlegel, K. Maxeiner, B. Weber, M. Barz, M.A. Schroer, C. E. Blanchet, D.I. Svergun, S. Ramishetti, D. Peer, P. Langguth, U. Sahin, H. Haas, Polysarcosine-functionalized lipid nanoparticles for therapeutic mRNA delivery, ACS Appl. Nano Mater. 3 (2020) 10634–10645.
[32] K.K. Gill, A. Kaddoumi, S. Nazzal, PEG-lipid micelles as drug carriers: physiochemical attributes, formulation principles and biological implication, J. Drug Target. 23 (2015) 222–231.
[33] O.K. Nag, V. Awasthi, Surface engineering of liposomes for stealth behavior, Pharmaceutics 5 (2013) 542–569.
[34] K. Nakamura, K. Yamashita, Y. Itoh, K. Yoshino, S. Nozawa, H. Kasukawa, Comparative studies of polyethylene glycol-modified liposomes prepared using different PEG-modification methods, Biochim. Biophys. Acta 2012 (1818) 2801–2807.
[35] J.-M. Rabanel, P. Hildgen, X. Banquy, Assessment of PEG on polymeric particles surface, a key step in drug carrier translation, J. Control. Release 185 (2014) 71–87.
[36] H. Ren, Y. He, J. Liang, Z. Cheng, M. Zhang, Y. Zhu, C. Hong, J. Qin, X. Xu, J. Wang, Role of liposome size, surface charge, and PEGylation on rheumatoid arthritis targeting therapy, ACS Appl. Mater. Interfaces 11 (2019) 20304–20315.
[37] K. Remaut, B. Lucas, K. Braeckmans, J. Demeester, S.C. De Smedt, Pegylation of liposomes favours the endosomal degradation of the delivered phosphodiester oligonucleotides, J. Control. Release 117 (2007) 256–266.
[38] N. Djedovič, R. Ferdani, E. Harder, J. Pajewska, R. Pajewski, M.E. Weber, P. H. Schlesinger, G.W. Gokel, The C- and N-terminal residues of synthetic heptapeptide ion channels influence transport efficacy through phospholipid bilayers, New J. Chem.=Nouv. J. Chim. 29 (2005) 291–305.
[39] C. Fetsch, A. Grossmann, L. Holz, J.F. Nawroth, R. Luxenhofer, Polypeptoids from N-Substituted Glycine N-Carboxyanhydrides: Hydrophilic, Hydrophobic, and Amphiphilic Polymers with Poisson Distribution, Macromolecules 44 (2011) 6746–6758.
[40] J. Ulbricht, R. Jordan, R. Luxenhofer, On the biodegradability of polyethylene glycol, polypeptoids and poly(2-oxazoline)s, Biomaterials 35 (2014) 4848–4861.
[41] A. Birke, D. Huesmann, A. Kelsch, M. Weilbächer, J. Xie, M. Bros, T. Bopp, C. Becker, K. Landfester, M. Barz, Polypeptoid-block-polypeptide copolymers: synthesis, characterization, and application of amphiphilic block copolypept(o)ides in drug formulations and miniemulsion techniques, Biomacromolecules 15 (2014) 548–557.
[42] S.W. Jin, D. Beis, T. Mitchell, J.N. Chen, D.Y. Stainier, Cellular and molecular analyses of vascular tube and lumen formation in zebrafish, Development 132 (2005) 5199–5209.
[43] C. Muhl, M. Conrad, D. Unthan, M. Barz, Synthesis and characterization of bisalkylated polysarcosine-based lipopolymers, Eur. Polym. J. 120 (2019).
[44] C. Kappel, C. Seidl, C. Medina-Montano, M. Schinnerer, I. Alberg, C. Leps, J. Sohl, A.-K. Hartmann, M. Fichter, M. Kuske, J. Schunke, G. Kuhn, I. Tubbe, D. Paßlick, D. Hobernik, R. Bent, K. Haas, E. Montermann, K. Walzer, M. Diken, M. Schmidt, R. Zentel, L. Nuhn, H. Schild, S. Tenzer, V. Mailänder, M. Barz, M. Bros, S. Grabbe, Density of conjugated antibody determines the extent of fc receptor dependent capture of nanoparticles by liver sinusoidal endothelial cells, ACS Nano 15 (2021) 15191–15209.
[45] L. Viitala, S. Pajari, L. Gentile, J. Määttä, M. Gubitosi, J. Deska, M. Sammalkorpi, U. Olsson, L. Murtomäki, Shape and Phase Transitions in a PEGylated Phospholipid System, Langmuir 35 (2019) 3999–4010.
[46] M.L. Immordino, F. Dosio, L. Cattel, Stealth liposomes: review of the basic science, rationale, and clinical applications, existing and potential, Int. J. Nanomedicine 1 (2006) 297–315.
[47] Y. Hattori, K. Tamaki, S. Sakasai, K.I. Ozaki, H. Onishi, Effects of PEG anchors in PEGylated siRNA lipoplexes on in vitro genesilencing effects and siRNA biodistribution in mice, Mol. Med. Rep. 22 (2020) 4183–4196.
[48] S.S. Nunes, J. de Oliveira Silva, R.S. Fernandes, S.E.M. Miranda, E.A. Leite, M.A. de Farias, R.V. Portugal, G.D. Cassali, D.M. Townsend, M.C. Oliveira, A.L.B. de Barros, PEGylated versus Non-PEGylated pH-sensitive liposomes: new insights from a comparative antitumor activity study, Pharmaceutics 14 (2022).
[49] Y. Li, J. Wang, Y. Gao, J. Zhu, M.G. Wientjes, J.L.S. Au, Relationships between liposome properties, cell membrane binding, intracellular processing, and intracellular bioavailability, AAPS J. 13 (2011) 585–597.
[51] Y. Sadzuka, K. Kishi, S. Hirota, T. Sonobe, Effect of Polyethyleneglycol (PEG) Chain on Cell Uptake of PEG-Modified Liposomes, J. Liposome Res. 13 (2003) 157–172.
[52] R.C. Ryals, S. Patel, C. Acosta, M. McKinney, M.E. Pennesi, G. Sahay, The effects of PEGylation on LNP based mRNA delivery to the eye, PLoS One 15 (2020), e0241006.
[53] S. Sieber, P. Grossen, P. Detampel, S. Siegfried, D. Witzigmann, J. Huwyler, Zebrafish as an early stage screening tool to study the systemic circulation of nanoparticulate drug delivery systems in vivo, J. Control. Release 264 (2017) 180–191.
[54] N.-J.K. Dal, A. Kocere, J. Wohlmann, S. Van Herck, T.A. Bauer, J. Resseguier, S. Bagherifam, H. Hyldmo, M. Barz, B.G. De Geest, F. Fenaroli, Zebrafish embryos allow prediction of nanoparticle circulation times in mice and facilitate quantification of nanoparticle–cell, Interactions 16 (2020) 1906719.
[55] F. Campbell, F.L. Bos, S. Sieber, G. Arias-Alpizar, B.E. Koch, J. Huwyler, A. Kros, J. Bussmann, Directing nanoparticle biodistribution through evasion and exploitation of Stab2-dependent nanoparticle uptake, ACS Nano 12 (2018) 2138–2150.
[56] M. Morsch, R. Radford, A. Lee, E. Don, A. Badrock, T. Hall, N. Cole, R. Chung, In vivo Characterization of Microglial Engulfment of Dying Neurons in the Zebrafish Spinal Cord 9, 2015.
[57] R.W. Friedrich, G.A. Jacobson, P. Zhu, Circuit neuroscience in zebrafish, Curr. Biol. 20 (2010) R371–R381.
[58] M. Stobb, J.M. Peterson, B. Mazzag, E. Gahtan, Graph theoretical model of a sensorimotor connectome in zebrafish, PLoS One 7 (2012), e37292.
[59] J. Kanungo, S. Lantz, M.G. Paule, In vivo imaging and quantitative analysis of changes in axon length using transgenic zebrafish embryos, Neurotoxicol. Teratol. 33 (2011) 618–623.
[60] L.J. Caldwell, N.O. Davies, L. Cavone, K.S. Mysiak, S.A. Semenova, P. Panula, J. D. Armstrong, C.G. Becker, T. Becker, Regeneration of Dopaminergic Neurons in Adult Zebrafish Depends on Immune System Activation and Differs for Distinct Populations 39, 2019, pp. 4694–4713.
[61] M. Kunst, E. Laurell, N. Mokayes, A. Kramer, F. Kubo, A.M. Fernandes, D. Forster, M. Dal Maschio, H. Baier, A cellular-resolution atlas of the larval zebrafish brain, Neuron 103 (2019) 21–38 e25.